Archives of Hydro-Engineering and Environmental Mechanics
Vol. 50 (2003), No. 4, pp. 401–413

Mixing in Strongly Stratified Bottom Cavities of Estuaries: an Experimental Study

Yarko Niño, Juan Francisco Miranda

Department of Civil Engineering, University of Chile Casilla 228-3, Santiago, Chile,
Principal author email: ynino@ing.uchile.cl

(Received June 27, 2003; revised Otober 02, 2003)

Abstract

Results of an experimental study on the mixing characteristics of the stratified flow inside bottom cavities in salt wedge estuaries are presented and discussed. The experiments were conducted in a laboratory flume where a cavity was formed by placing two consecutive sills over the channel bottom. The cavity was filled with a bottom layer of saline water with a sharp density interface. A constant fresh water discharge was supplied at the upstream end of the flume. An ADV and a fast conductivity probe were used to measure the turbulence and salinity structure inside the cavity. Flow visualizations were made, in addition, to keep track of the position of the density interface inside the cavity. The density interface tilts in the downstream direction with a slope that increases as the local densimetric Froude number, Fr_d, increases. This slope can be reasonably estimated from a linear analysis of the response of the 2-layer stratified fluid to an interfacial shear stress. The entrainment velocity, or rate of interface deepening due to mixing, decreases as Fr_d increases, which appears to be the consequence of a decreasing mixing efficiency related to the tilting of the interface. The present entrainment velocity data compares well with existing experimental data and models, validating the latter on an extended range of relevant parameters. By scaling these results to a prototype such as the Valdivia Estuary in Chile, it is concluded that purging of the saline water trapped inside of bottom cavities cannot be completed during a tidal period.

Key words: stratified flows, mixing, estuaries, experimental methods, Acoustic Doppler Velocimetry

List of Symbols

The following symbols have been used in the paper:

c_{fi} – internal friction coefficient,
$D = h_1 + h_2 - H$ – flow depth at the tip of the sills,
$Fr_d = q_f/(g\phi h_1^3)^{1/2}$ – densimetric Froude number,
H – sills height,

h_1 – thickness of the upper layer,

h_2 – thickness of the bottom layer,

K – D & A's mixing efficiency coefficient,

L – top length of the cavity,

Q_f – fresh water discharge,

q_f – freshwater discharge per unit width,

$Re = q_f/\nu$ – flow Reynolds number,

R_f – bulk mixing efficiency coefficient,

R'_f – local mixing efficiency coefficient,

$r_p = T_p/T_d$ – purging coefficient,

$r_T = T_r/T_d$ – retention time to tidal period ratio,

S_i – interfacial slope,

T_d – tidal period,

TKE_i – turbulent kinetic energy at the density interface,

$T_p = H/u_e$ – purge time,

$T_r = V_c/Q_f$ – retention time within the cavity,

U_1 – depth averaged velocity in upper layer,

$u_1 = q_f/h_1$ – overflow velocity,

U_2 – depth averaged velocity in lower layer,

u_e – entrainment velocity,

V_c – volume of the cavity,

w_{RMSi} – RMS of the vertical fluctuating velocity component at the density interface,

$\phi = (\rho_2 - \rho_1)/\rho_1$ – relative density difference between upper and bottom layers,

ν – kinematic viscosity,

ρ_1 – density of upper layer,

ρ_2 – density of bottom layer,

τ_f – bottom shear stress,

τ_i – interfacial shear stress,

τ_s – surface shear stress,

ξ_1 – free surface vertical displacement,

ξ_2 – interface vertical displacement.

1. Introduction

Estuaries usually have an irregular bathymetry with a quasi-periodic spatial distribution of pools or depressions of the channel bottom. The interaction between these pools and the flow in the estuary is particularly relevant in the presence of a salt wedge, as the tide forces periodical longitudinal excursions of the wedge along the estuary. During the ebb cycle, when the salt wedge recedes towards the ocean, saline water can remain trapped in the bottom pools of the estuary (Debler and Armfield 1997). The case of the Valdivia Estuary in Chile is a good example of this situation (Imberger and Thompson 1994). During the ebb cycle, fresh water flows into the pools and eventually mixes with the saline water. However, the stratification of the pools exerts resistance to mixing, avoiding the complete purging of the trapped saline water. The water in the pools often remains stably stratified after a number of tidal cycles and does not circulate sufficiently to allow adequate aeration. The pools can become hypoxic with negative consequences from the point of view of water quality in the system (Armfield and Debler 1993, Kurup and Hamilton 2002). Insight into the mixing dynamics between fresh and saline water inside the pools is needed in order to develop effective remediation measures to the problem. This paper reports results of an experimental study conducted with this aim, providing new data and information regarding the mixing characteristics of the stratified flow inside bottom cavities in a salt wedge situation. The experimental results presented here complement previous experimental results by Armfield and Debler (1993) and Debler and Armfield (1997), providing more detailed information regarding the turbulent structure of the flow inside the cavities and validating, in an extended range of the relevant parameters, some aspects of the models proposed by these researchers. Parts of this paper were presented during the Fifth International Conference on Hydro-Science and Engineering in Warsaw, Poland.

2. Experimental Study

The experiments were conducted in a flume 10 m long and 0.4 m wide. A cavity, representing a bottom pool in an estuary was formed near the downstream end, by placing two consecutive sills over the channel bottom. The sills were of a sinusoidal shape, with a height $H = 0.1$ m, length and width of 0.4 m, and were separated by a distance of 0.26 m at their base (Fig. 1). The cavity was filled with a bottom layer of saline water, of thickness h_2, with a sharp density interface. A constant fresh water discharge was supplied at the upstream end of the flume. A tilting gate was used at the downstream end to control the flow depth and consequently, the thickness of the layer of fresh water on top of the saline water within the cavity, h_1. An acoustic doppler velocimeter was used to obtain vertical profiles of three components of the velocity of the flow inside the cavity. Simultaneous measurements of water conductivity were made with a fast conductivity probe.

Flow visualizations were made, in addition, to keep track of the position of the density interface inside the cavity during the experiments. For this purpose the saline water was dyed with rodamine. The flow visualizations were recorded in digital video. Selected images of each experiment were analyzed in a computer to quantify the response of the density interface and estimate the amount of saline water purged from the cavity as a function of time, due to mixing induced by the fresh water overflow. More details about the experimental study can be found in Miranda (2001).

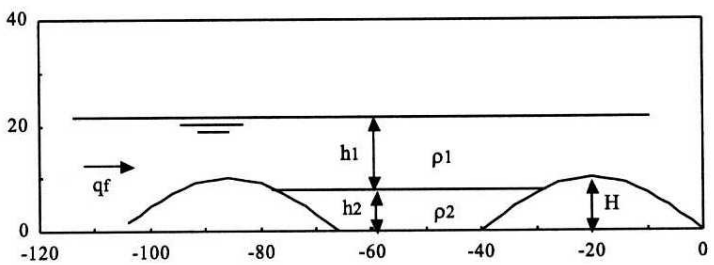

Fig. 1. Geometry of the cavity and definition of variables. Dimensions are in cm

Different experimental conditions were tested by changing the fresh water discharge per unit width, q_f, and the thickness of saline water inside the cavity. The relative density difference between saline and fresh water, $\phi = (\rho_2 - \rho_1)/\rho_1$, was kept constant at a value of 0.00115. The total depth, $h_1 + h_2$, was also held approximately constant and equal to about 0.225 m. Flow Reynolds numbers, Re $= q_f/\nu$, where ν is the kinematic viscosity of the fresh water, were in the range of 2000 to 7000. A summary of the experimental conditions is given in Table 1.

Table 1. Experimental conditions

q_f (cm^2/s)	Fr_d^2	h_1 (cm)	h_2 (cm)	Re
21.0	0.18	13.0	9.0	2105
21.0	0.18	12.9	9.1	2105
28.6	0.33	13.0	9.0	2860
37.3	0.35	15.2	7.8	3727
41.2	0.53	14.2	7.8	4122
48.6	0.50	16.1	6.4	4857
48.6	0.44	16.8	6.2	4857
58.6	0.49	18.4	4.6	5861
60.2	0.58	17.7	5.3	6019
70.7	0.65	18.9	3.1	7071

3. Analysis of Experimental Results

3.1. The Response of the Density Interface

As soon as the discharge of fresh water is established, the density interface inside the cavity responds by tilting in the downstream direction. This behaviour was not reported in previous experiments by A & D (Armfield and Debler 1993) and D & A (Debler and Armfield 1997). Probably, because of the interface tilting, there was not significant splash of the saline water in the downstream end of the cavity at the beginning of the experiment, as is described by D & A. In some cases, a wave front or crest was observed to form upstream and to travel along the cavity, finally striking its far wall. This crest has been described by A & D as being associated with the development of a vortex layer at the entrance of the cavity and is formed by the rolling up of the interface in a vortex that is advected along by the overflow. In the present experiments the crest striking the downstream wall did not result in the purging of saline water from the cavity, as described by A & D, as the tilting of the interface lowered it enough in the downstream end of the cavity for the saline water to reach the top of the sill. Considering these observations, the purging of saline water from the cavity in the present experiments is associated mainly with turbulent mixing across the density interface, occurring along the cavity.

Quantitative analysis of flow visualizations yielded mean values of the slope of the density interface for each experimental condition. Values of the interface slope, S_i, are plotted in Fig. 2 as a function of the densimetric Froude number, Fr_d defined as: $Fr_d^2 = q_f^2/(g\ \phi\ h_1^3)$, where g denotes gravity acceleration. The absolute value of S_i increases as Fr_d increases. It is postulated that the downstream tilting of the density interface is related to a local negative value of the shear stress at the interface. In fact, a linearization of the equations of motion in a two-layer stratified fluid yields (Spiegel and Imberger 1980, Heaps 1984):

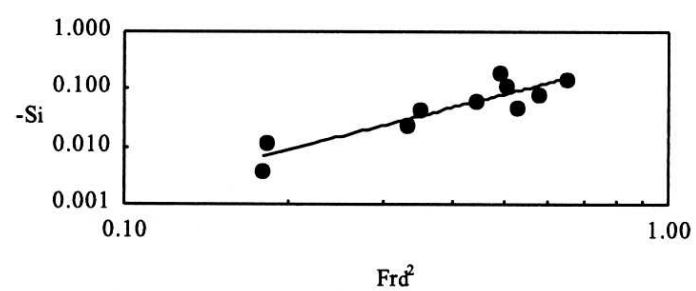

Fig. 2. Interface slope as a function of the densimetric Froude number. Line is a power law best fit to the data

$$\frac{\partial U_1}{\partial t} + g\,\frac{\partial \xi_1}{\partial x} = \frac{1}{\rho_1 h_1}(\tau_s - \tau_i), \tag{1}$$

$$\frac{\partial U_2}{\partial t} + g\,\frac{\rho_1}{\rho_2}\,\frac{\partial \xi_1}{\partial x} + g\,\frac{(\rho_2 - \rho_1)}{\rho_2}\,\frac{\partial \xi_2}{\partial x} = \frac{1}{\rho_2 h_2}(\tau_i - \tau_f), \tag{2}$$

where U_1 and U_2 denote depth averaged velocities in upper and lower layers, respectively, ξ_1 and ξ_2 denote free surface and interface vertical displacements, respectively, defined positive upwards, and τ_s, τ_i, and τ_f denote the shear stress values at the free surface, density interface and bottom surface of the cavity, respectively. In a steady state situation, with $\tau_s = 0$ and neglecting τ_f, the slope of the density interface is given by:

$$S_i = \frac{\partial \xi_2}{\partial x} = \frac{\tau_i}{g\,(\rho_2 - \rho_1)}\,\frac{(h_1 + h_2)}{h_1 h_2}, \tag{3}$$

which indicates that a negative interface slope is related to a negative value of τ_i. By introducing the internal friction coefficient, c_{fi}, such that:

$$\tau_i = -\,c_{fi}\,\rho_1\,\frac{q_f^2}{h_1^2} \tag{4}$$

the following relationship is obtained:

$$S_i = -\,c_{fi}\,Fr_d^2\left(1 + \frac{h_1}{h_2}\right). \tag{5}$$

Measurements of the mean velocity profile inside the cavity, together with values of the turbulent shear stress were used to obtain estimations of the interface shear stress as the sum of viscous and turbulent stresses. Associated values of c_{fi} are in the range of from 0.02 to 0.04 for the present experimental conditions. A comparison of experimental values of S_i and those given by (5) for corresponding experimental conditions is presented in Fig. 3. The present model does a reasonable job in explaining the observations of S_i. Discrepancies can be explained by experimental errors in the estimation of c_{fi} and other effects, such as longitudinal pressure gradients inside the cavity related to flow separation at the entrance.

3.2. Turbulence and Salinity Structure inside the Cavity

Examples of measurements of velocity and density structure inside the cavity are shown in Figs. 4 to 6, corresponding to the value $Fr_d^2 = 0.33$. Mean dimensionless velocity profiles near the upstream sill show negligible motion in the saline layer, however, some distance downstream, vertical turbulent diffusion of streamwise momentum creates a two-cell circulation structure inside the cavity, even though the circulation in the bottom layer is extremely weak (Fig. 4). Interface tilting is

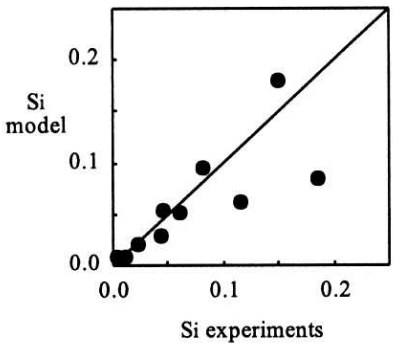

Fig. 3. Comparison between experimental values of S_i and those given by (5)

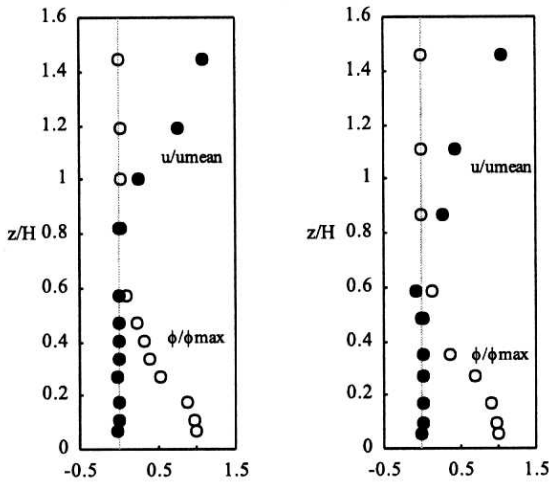

Fig. 4. Dimensionless vertical profiles of mean streamwise flow velocity, u, and relative density difference. The vertical coordinate z is made dimensionless with the sill height; u is made dimensionless with the mean velocity of the flow over the sill, u_{mean}. Left profiles correspond to a distance $x = 0$ m, measured from the base of the upstream sill. Right profiles correspond to a distance $x = 0.13$ m

evident from the relative density difference profiles in Figs. 4 and 5. Maximum RMS values of ϕ occur at the density interface (Fig. 5), associated to internal wave activity. On the contrary, RMS values of the vertical fluctuating velocity component are minimum at the density interface (Fig. 6). Vertical profiles of turbulent kinetic energy, TKE, near the upstream sill exhibit a maximum some distance over the top of the sill, associated with the overflow of fresh water (Fig. 6). This maximum is diffused vertically along the cavity, and the corresponding profiles become more uniform downstream. Values of the TKE within the saline layer are about 15 to 40% of the maximum TKE values associated with the fresh-water

overflow, decreasing in the downstream direction as the result of the tilting of the density interface (Fig. 6).

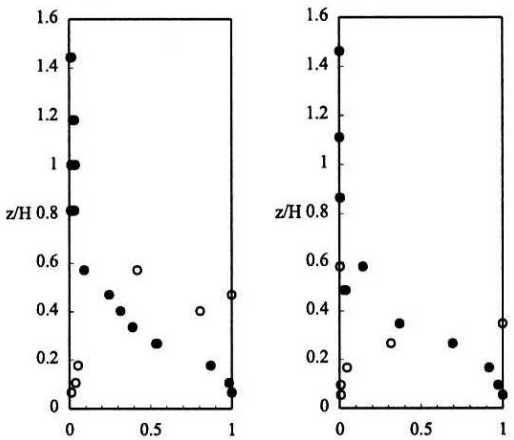

Fig. 5. Dimensionless vertical profiles of mean and RMS values of the relative density difference. Black circles correspond to values of ϕ made dimensionless with the maximum value of ϕ. White circles correspond to the RMS values of ϕ made dimensionless with the maximum RMS value of ϕ. Left profiles correspond to a distance $x = 0$ m, measured from the base of the upstream sill. Right profiles correspond to a distance $x = 0.13$ m

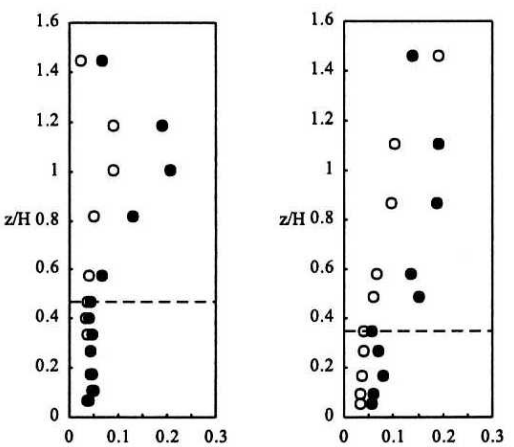

Fig. 6. Dimensionless vertical profiles of TKE and the RMS values of the vertical fluctuating velocity component, w_{RMS}. Black circles correspond to values of w_{RMS} made dimensionless with u_{mean}. White circles correspond to the TKE values made dimensionless with u^2_{mean}. Dashed lines indicate the position of the density interface. Left profiles correspond to a distance $x = 0$ m, measured from the base of the upstream sill. Right profiles correspond to a distance $x = 0.13$ m

3.3. Mixing

The rate of deepening of the density interface, or entrainment velocity u_e, associated with turbulent mixing along the cavity, was estimated from the analysis of flow visualizations. The entrainment velocity, made dimensionless with the overflow velocity $u_1 = q_f/h_1$, decreases as Fr_d^2 increases (Fig. 7). A power law best fit yields:

$$\frac{u_e}{u_1} = 0.0009\ (Fr_d^2)^{-0.337}. \tag{6}$$

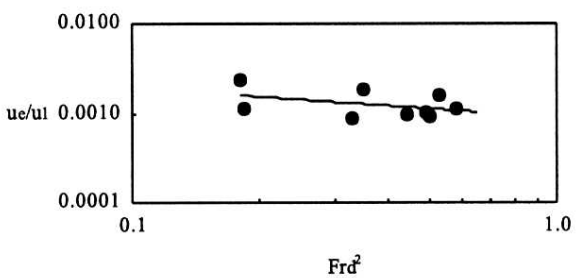

Fig. 7. Dimensionless entrainment velocity as a function of the densimetric Froude number. Line represents Eqn. (6)

This behaviour is contrary to typical entrainment relationships, for which the dimensionless entrainment velocity increases with the densimetric Froude number (e.g. Christodoulou 1986).

An analysis based on the concept of mixing efficiency (e.g. Hopfinger 1987, Debler and Armfield 1997, Peltier and Caulfield 2003) is used to develop a simple model to estimate the entrainment velocity inside the cavity. Assuming that mixing increases the potential energy inside the cavity at the expense of the kinetic energy of the overflow, the following relationship is proposed:

$$\frac{1}{2}\, g\ (\rho_2 - \rho_1)\, u_e\, h_1^2 = R_f\, \frac{1}{2}\, \rho_1\, q_f\, u_1^2, \tag{7}$$

which expresses that the rate of increase of potential energy associated with mixing is balanced by part of the flow of kinetic energy of the freshwater overflow, and R_f denotes a bulk mixing efficiency coefficient. From (7) the dimensionless entrainment velocity is given by:

$$\frac{u_e}{u_1} = R_f\ Fr_d^2, \tag{8}$$

which implies that u_e/u_1 is directly proportional to Fr_d^2. Comparison with experimental results leads to the conclusion that R_f is a function of the densimetric

Froude number. The present data indicate that the bulk mixing efficiency decreases as Fr_d^2 increases (Fig. 8). This conforms with the fact that the slope of the density interface increases as Fr_d^2 increases (Fig. 2) which implies that the interface gets progressively hidden within the cavity as this parameter increases, thus becoming less exposed to high values of the TKE.

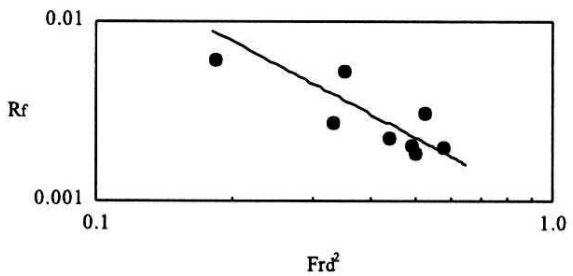

Fig. 8. Bulk mixing efficiency coefficient as a function of the densimetric Froude number. Line represents a power law best fit to the data

A local instead of a bulk version of the mixing efficiency coefficient is proposed (Hopfinger 1987), given by the following relationship:

$$R_f' = \frac{g\,\phi\,u_e\,h_1}{TKE_i\,w_{RMSi}}, \tag{9}$$

where the denominator corresponds to an estimated value of the vertical flux of TKE towards the density interface, given by the product of the values of TKE and the RMS vertical fluctuating velocity component at the density interface, TKE_i and w_{RMSi}, respectively. Values of R_f' are estimated using the present turbulence measurements. This local value of the mixing efficiency coefficient, as the bulk value R_f, also decreases as a function of Fr_d^2 (Fig. 9). Nonetheless, the mixing efficiency estimated as in (9) is much larger than the bulk version R_f, reaching values of about 10 to 55%.

Comparison of the present entrainment velocity data with similar experimental data of D & A (Debler and Armfield, 1997) is presented in Fig. 10. Cavities in D & A had rectangular and trapezoidal shapes. D & A's data in Fig. 10 corresponds to a trapezoidal cavity with an aspect ratio $L/H = 6.9$, where L is the top length of the cavity. The present data corresponds to $L/H = 6.6$, where L denotes the distance between the top of the sills (Fig. 1). D & A's entrainment relationship, obtained from arguments based on a mixing efficiency coefficient similar to those used to derive (8), is also plotted in Fig. 10. D & A's relationship is given by:

$$\frac{u_e/u_1}{Fr_c^2} = K\left\{\left(1-\frac{h_2}{H}\right)\left(1+\frac{H}{D}-\frac{h_2}{H}\right)^2\right\}^{-1}, \tag{10}$$

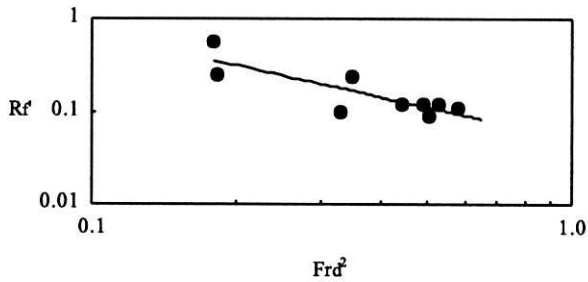

Fig. 9. Local mixing efficiency coefficient as a function of the densimetric Froude number. Line represents a power law best fit to the data

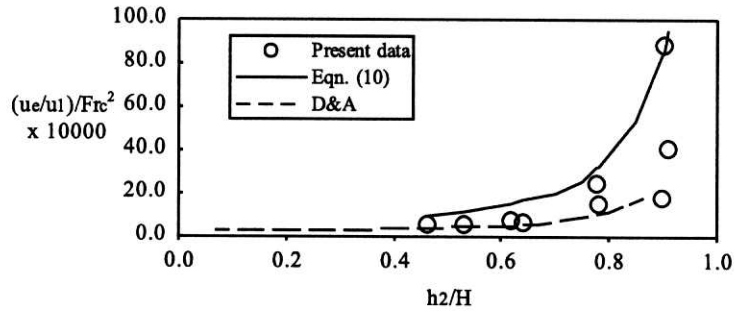

Fig. 10. Comparison between A & D's entrainment relationship, their experimental data and present data. Dashed line represents the trend defined by A & D actual data

where Fr_c represents a densimetric Froude number for the cavity, defined as:

$$Fr_c^2 = Fr_d^2 \frac{h_1^3}{D^2 H}, \tag{11}$$

K denotes a kind of mixing efficiency coefficient and $D = h_1 + h_2 - H$. D & A proposed the value $K = 0.001$ for (10) to fit their experimental data. This same value is used in Fig. 10. The present data fit A & D's data and also Eq. (10) fairly well, validating the latter in a wider range of values of h_2/H, particularly as this ratio tends to unity.

4. Scaling of Present Results to the Valdivia Estuary in Chile

It is interesting to use the present experimental results to estimate mixing rates within bottom cavities in a real estuary and to assess the purging potential of a fresh-water overflow during the tidal ebb cycle. Miranda (2001), based on field information reported by Imberger and Thompson (1994), applied the present results to the Valdivia Estuary in Chile, finding that the present experimental range of densimetric Froude numbers matches fairly well those observed in the Valdivia estuary. The complete purge time for a particular cavity of depth H was

estimated as: $T_p = H/u_e$. To assess whether complete purging is possible within a tidal period, T_d, the purging coefficient is defined as $r_p = T_p/T_d$. If $r_p > 1/2$, then complete purging would not be possible within the tidal ebb cycle. Proper scaling is needed in order to estimate values of T_d associated with the present experimental conditions. This is done by assuming that the experimental values of the ratio $r_T = T_r/T_d$ correspond to those observed in the field situation, where T_r denotes the retention time within the cavity given by: $T_r = V_c/Q_f$, where V_c denotes the volume of the cavity and Q_f the fresh water discharge. Several bottom cavities were identified in a reach of 25 km of the Valdivia estuary (Fig. 11). Values of r_T vary in the range 0.09 to 0.43. Values of the purging coefficient estimated as: $r_p = (T_p r_T)/T_r$ using the present experimental values of T_p and T_r and the field values of r_T are in the range of from about 10 to 100. This shows that purging of saline water within bottom cavities of the Valdivia estuary cannot be completed during a tidal period, with probable negative consequences from the point of view of water quality within the cavities.

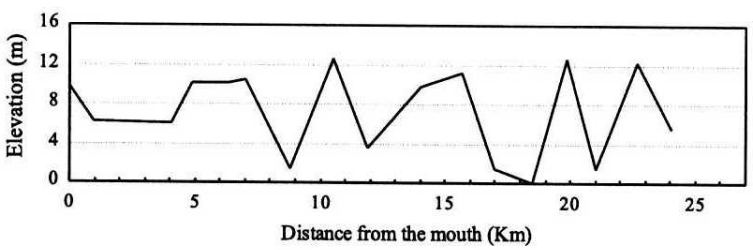

Fig. 11. Bathymetry of Valdivia Estuary. Imberger and Thompson (1994)

5. Conclusions

The present experimental results show that the density interface inside the cavity responds to the fresh water overflow by tilting in the downstream direction with a slope that increases as Fr_d increases. This slope can be reasonably estimated from a linear analysis of the response of the 2-layer stratified fluid to an interfacial shear stress. The entrainment velocity, or rate of interface deepening due to mixing, decreases as Fr_d increases, and this appears to be a consequence of a corresponding decreasing mixing efficiency, related to the tilting of the density interface. The present entrainment velocity data compares well with A & D's experimental data for similar values of the aspect ratio of the cavity, and validates the entrainment relationship proposed by them on a wider range of values of the h_2/H ratio. By scaling these results to a prototype such as the Valdivia Estuary in Chile, it is concluded that purging of the saline water trapped inside bottom cavities cannot be completed during a tidal period.

Acknowledgments

The authors gratefully acknowledge financial support given by FONDECYT through project 1010483 and the Department of Civil Engineering of the University of Chile.

References

Armfield S. W., Debler W. (1993), Purging of Density Stabilized Basins, *Int. J. Heat Mass Transfer*, Vol. 36, No. 2, 519–530.

Christodoulou G. C. (1986), Interfacial Mixing in Stratified Flows, *J. Hydr. Research*, Vol. 24, No. 2, 77–92.

Debler W., Armfield S. W. (1997), The Purging of Saline Water from Rectangular and Trapezoidal Cavities by an Overflow of Turbulent Sweet water, *J. Hydr. Research*, Vol. 35, No. 1, 43–62.

Heaps N. S. (1984), *Hydrodynamics of Lakes*, K. Hutter, editor, Springer-Verlag.

Hopfinger E. J. (1987), Turbulence in Stratified Fluids: A Review, *J. Geoph. Res.*, Vol. 92, No. 5, 5287–5303.

Imberger J., Thompson C. (1994), *Report on the Valdivia Estuary, Chile*, Centre for Water Research, The University of Western Australia. WP 932 JI.

Kurup R. G., Hamilton D. P. (2002), Flushing of Dense Hypoxic Water from a Cavity of the Swan River Estuary, Western Australia, *Estuaries*, 25(5), 908–915.

Miranda J. F. (2001), *Theoretical and Experimental Study on Bathymetry Effects upon Salinity Intrusion in Stratified Estuaries*, Undergraduate thesis, Dept. of Civil Engineering, University of Chile (in Spanish).

Peltier W. R., Caulfield C. P. (2003), Mixing Efficiency in Stratified Shear Flows, *Annu. Rev. Fluid Mech.*, 35, 135–167.

Spiegel R. H., Imberger J. (1980), The Classification of Mixed-Layer Dynamics in Lakes of Small to Medium Size, *J. Phys. Oceanogr.*, 10, 1104–1121.